# Tidal interactions and disruptions of giant planets on highly eccentric orbits

Joshua A. Faber *, Frederic A. Rasio, Bart Willems

*Northwestern University, Department of Physics and Astronomy, Evanston, IL 60208, USA*

## Abstract

We calculate the evolution of planets undergoing a strong tidal encounter using smoothed particle hydrodynamics (SPH), for a range of periastron separations. We find that outside the Roche limit, the evolution of the planet is well-described by the standard model of linear, non-radial, adiabatic oscillations. If the planet passes within the Roche limit at periastron, however, mass can be stripped from it, but in no case do we find enough energy transferred to the planet to lead to complete disruption. In light of the three new extrasolar planets discovered with periods shorter than two days, we argue that the shortest-period cases observed in the period-mass relation may be explained by a model whereby planets undergo strong tidal encounters with stars, after either being scattered by dynamical interactions into highly eccentric orbits, or tidally captured from nearly parabolic orbits. Although this scenario does provide a natural explanation for the edge found for planets at twice the Roche limit, it does not explain how such planets will survive the inevitable expansion that results from energy injection during tidal circularization.
© 2004 Elsevier Inc. All rights reserved.

*Keywords:* Planetary dynamics; Tides, solid body; Extrasolar planets; Jovian planets

## 1. Introduction

Approximately 17% of extrasolar planets discovered to date can be classified as "hot Jupiters," gas giant planets in very tight orbits (with orbital periods of $< 10$ days) around solar-like stars (Sasselov, 2003; Mayor et al., 2004; Bouchy et al., 2004; Konacki et al., 2004). Of these 21 planets, 17 have periods of less than five days. In this context, strong tidal interactions between a giant planet and its central star have become an important problem. Many studies have focused on understanding the mechanisms and consequences of tidal *dissipation* in these systems (Rasio et al., 1996; Lubow et al., 1997; Ford et al., 1999; Gu et al., 2003; Sasselov, 2003; Ivanov and Papaloizou,

2004a, 2004b; Ogilvie and Lin, 2004). Here instead we examine *dynamical* interactions, in which a giant planet on a nearly-parabolic orbit passes very close to the central star. There are at least two scenarios where such interactions would occur. The first is the scattering scenario for explaining the high eccentricities of extrasolar planets (Rasio and Ford, 1996; Weidenschilling and Marzari, 1996; Lin and Ida, 1997; Ford et al., 2001; Marzari and Weidenschilling, 2002; Adams and Laughlin, 2003). In this scenario, protoplanetary systems containing several giant planets of comparable masses become dynamically unstable, leading to strong scattering between planets. Planets scattered inward may sometimes undergo strong tidal interactions with the central star, perhaps even leading to capture onto a much shorter-period circular orbit. In the second scenario, discussed recently by Gaudi (2003), "free-floating" planets in the dense cluster environments where most stars are formed would be tidally captured by protostars, in a manner reminiscent of the old tidal-capture scenario for forming compact binaries in glob-

* Corresponding author. Current address: University of Illinois at Urbana-Champaign, Department of Physics, Loomis Laboratory, 1110 W. Green St., Urbana, IL 61801, USA.

*E-mail address:* jfaber@uiuc.edu (J.A. Faber).

ular clusters (Fabian et al., 1975; Press and Teukolsky, 1977; Lee and Ostriker, 1986). As far as the close encounter is concerned, the only difference between these two scenarios is whether the nearly-parabolic orbit of the incoming planet is in fact slightly hyperbolic or elliptic.

In this paper we study the strong tidal interaction between a giant planet and a solar-like star using 3-D numerical hydrodynamic calculations. We focus on encounters with periastron separations of a few solar radii, which can lead to significant dissipation of orbital energy and mass loss. Since the details of the interaction are insensitive to the sign of the total energy, our results can be easily applied to the case of highly-eccentric elliptic orbits or low-energy hyperbolic orbits. The main questions we address concern the final fate of the planet following an interaction, and the possibility of an observational signature of strong tidal interactions. Surprisingly, we find that complete disruption of a Jupiter-like planet *outside* a solar-like star is never possible. If the interaction is close enough for the planet to be stripped of a significant fraction of its mass, its orbit always *gains* enough energy to become unbound (even if the initial orbit was bound). Even closer interactions would lead instead to a physical collision with the star. Observationally, hot Jupiters are confined to a region of parameter space that appears to follow closely a simple definition of the "tidal limit," shown in Fig. 1. Data points indicated by squares represent planets whose masses are known, since the mass function $M_P \sin i$ is constrained by the observation of transits. In all other cases, the mass shown represents a lower limit. The only planets that may fall within this limit, shown as triangles, have a much smaller mass, close to that of Neptune, and may well be structurally different from typical gas giants, as we discuss below.

It is not immediately clear that any common definitions of the tidal limit should be relevant here. Indeed, each is made under assumptions that are violated for highly eccentric planetary orbits, e.g., circular orbits and synchronized spins. We note one crucial fact about all the tidal limits discussed below, however. They all have the same physical scalings, with different coefficients, since the underlying dimensional analysis is the same for each.

The Hill radius, $r_H$, is defined in the context of the restricted three-body problem, and is commonly used in describing the orbits of a planet's satellites. Based on simple point-mass mechanics, it is found that a satellite can orbit stably around a planet of mass $M_P$ in a circular orbit of radius $a$ around a star of mass $M_*$ so long as its own orbit has a semimajor axis less than

$$r_H = a\left(\frac{M_P}{3(M_P + M_*)}\right)^{1/3} \approx 0.69 q^{1/3} a, \qquad (1)$$

where the latter relation holds for small mass ratios, i.e., $q = M_P/M_* \ll 1$. We note that what Gaudi (2003) refers to as the "Roche limit" is found by a brief calculation to be the Hill radius instead.
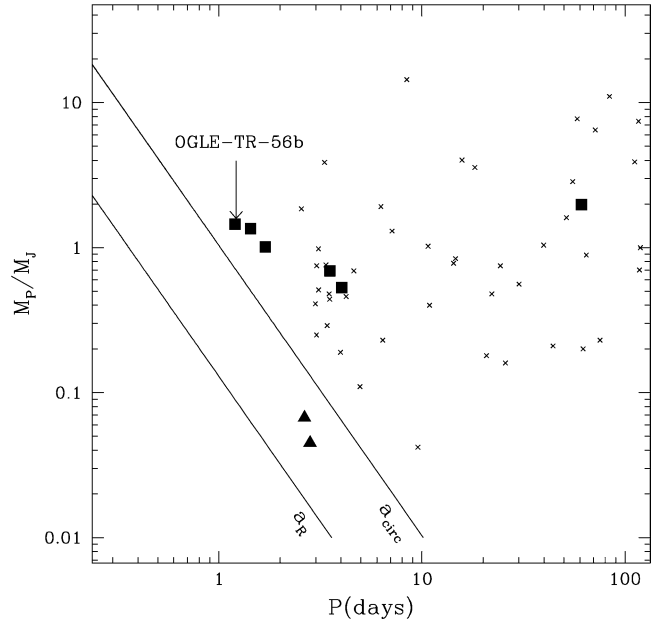


Fig. 1. Minimum mass $M_P \sin i$ versus orbital period for the current observed sample of planetary companions. OGLE-TR-56b is one of only six planets whose orbital inclination is known, all of which are marked by squares (for these, we show the actual mass). In all six cases, since the inclination is determined from eclipses, $i \geqslant 80°$. Triangles represent the possibly lower-mass "hot Neptunes," GJ436 b and 55 Cnc e, which may have a qualitatively different structure than the more massive planets on the figure. The Roche limit, $a_R$, defined via Eq. (3), is shown for a planet with a radius equal to that of Jupiter, as is the ideal circularization radius, $a_{circ}$, defined as an orbit with a separation twice as large as the Roche limit. Data are taken from the extra-solar planets catalog at http://www.obspm.fr/encycl/cat1.html.

The Roche lobe radius, $r_R$, is defined in terms of the classical stellar two-body problem. For two point masses in a circular orbit, there exists a critical equipotential surface in the rotating frame around each body, within which all corotating fluid is bound to it. This volume can be used to define a characteristic volume-averaged radius; for mass ratios much different than unity the Roche lobe around the less massive body is roughly spherical, with a cusp at the inner Lagrange point. In the limit of extremely small mass ratios ($q \ll 1$), the Roche lobe radius depends weakly on the compressibility of the less massive object (the primary is always assumed to be a point mass; see Lai et al., 1993, for an extended discussion). In most pioneering works (see, e.g., Jeans, 1919), it was assumed that the secondary was completely incompressible (corresponding to $n = 0$, or equivalently, $\Gamma \to \infty$). For this case, it was found that

$$r_R = 0.407 q^{1/3} a. \qquad (2)$$

Later, Paczyński (1971) considered the opposite limit, treating the secondary as a point-mass (corresponding to the infinitely *compressible* case). Based on tabulated results, he found that the Roche lobe radius is given by

$$r_R = 0.462 q^{1/3} a, \qquad (3)$$

and is almost exactly two-thirds the extent of the Hill radius. This is the definition of the Roche lobe radius that appears in Sasselov (2003), among many other sources, and will be the one used throughout this paper, for reasons we will explain in detail in Section 3. A related quantity we refer to regularly is the Roche limit $a_R$, defined as the critical separation where the planet fills its Roche lobe; it can be defined implicitly through the relation $r_R(a_R) \equiv R_P$.

Remarkably, we find that the present location of the tidal "edge" observed in Fig. 1 would be naturally explained if all planets, with the possible exception of the "hot Neptunes" shown as triangles, had been initially on highly eccentric orbits and later circularized *without significant mass or orbital angular momentum loss* at a distance approximately twice that of the Roche limit, which we will refer to as the "ideal circularization radius." Indeed, any initial orbit with extremely high eccentricity has a (specific) total angular momentum satisfying

$$j^2 \simeq 2GMr_p, \tag{4}$$

where $M$ is the total mass of the system and $r_p$ the periastron separation of the initial orbit. The final circular orbit, on the other hand, satisfies the condition

$$j^2 = GMa. \tag{5}$$

Assuming that tidal circularization occurs through dissipation of orbital energy but with no net loss of mass or angular momentum, and neglecting spin angular momentum, we conclude that the orbit will circularize at a separation $a \simeq 2r_p$. We show below why we believe the condition $r_p > r_R$ determines whether the planet remains in a bound orbit after the passage.

Our limits are placed under the assumption that these "hot Jupiters" have radii not very different from that of Jupiter, $R_J = 7.14 \times 10^9$ cm. This is consistent with current measurements for the three innermost planets found with OGLE ($R = 1.23 \pm 0.16R_J$ for OGLE-TR-56, $R = 1.08 \pm 0.07R_J$ for OGLE-TR-113, and $R = 1.15^{+0.80}_{-0.13}R_J$ for OGLE-TR-132; Sasselov, 2003; Torres et al., 2004; Mayor et al., 2004; Bouchy et al., 2004; Konacki et al., 2004), as well as recent theoretical calculations of the structure of giant planets with extremely short-period orbits (Burrows et al., 2004; Chabrier et al., 2004). If indeed the radii of some of these planets are slightly larger than that of Jupiter, as appears to be the case for HD 209458 with $R = 1.43 \pm 0.04R_J$, our conclusions remain unchanged, since the location of the "circularization separation" will move slightly to the right on our plot but maintain the same functional form.

The "hot Neptunes," GJ 436 b (Butler et al., 2004) and 55 Cnc e (McArthur et al., 2004) are significantly less massive than the other planets with periods $P < 3$ days, assuming they do not have improbably small inclination angles. The radii of these planets, however, are likely to be smaller than that of Jupiter, since an extended envelope would be blown away by radiation from the parent M dwarf; it has been

suggested that these planets may in fact be composed completely or in part of rock and ice (Butler et al., 2004) and may be the rocky remnant cores of gas giants which have lost significant amounts of mass to tidal heating or some other process (McArthur et al., 2004).

The scenario we investigate here differs in its predictions from those involving the slow inspiral of giant planets all the way to the tidal limit (as in many popular "migration scenarios"; see, e.g., Trilling et al., 1998; Gu et al., 2003). This long-term inspiral is expected to produce an "edge" at the Roche limit, not at a separation twice as large. In addition, it is unclear what mechanism would halt the orbital inspiral before the onset of Roche lobe overflow and mass loss from planets experiencing radial expansion from tidal heating. Various possibilities have been proposed which rely on the evacuation of the inner protoplanetary disk (Kuchner and Lecar, 2002) and tidal interactions involving the host star's own rotation (Ford et al., 1999), but it is unclear how any orbital model involving tidal decay would produce the currently observed "edge" further out.

One major caveat with highly eccentric orbits concerns the survival of the planet during orbital circularization. Previous calculations have indicated that as energy is injected into the planet during circularization, its radius should expand significantly, eventually leading to Roche lobe overflow (Bodenheimer et al., 2001, 2003; Gu et al., 2003, 2004). Of course, given that these same results were used to argue for a lack of planets with periods $P \lesssim 3$ days, it is fair to say that uncertainties still remain as to the evolution of planetary radii and separations through tidal dissipation and circularization. Of particular importance is determining the rate at which a planet can dissipate tidal energy, and the effect of the energy dissipation rate on the planet's radius. This process is complicated, and may depend sensitively on the rotation rate of the planet relative to the angular velocity during periastron passage (Ivanov and Papaloizou, 2004b). In any case, while we consider an examination of this matter to be an important step in understanding planetary orbital evolution, it is beyond the scope of this paper.

Our paper is organized as follows. In Section 2, we describe our Lagrangian SPH code, as well as the parameters used in our calculations. In Section 3, we detail the results of our calculations, looking in turn at the case where the planet passes outside of the Roche limit, and then the case where it passes within, since this is found to be crucial in determining the future evolution of the planet. In Section 4, we discuss how these results affect the current picture of the evolution of giant planets, and discuss further scenarios to which these results may be applied.

## 2. Method and approximations

All of our calculations were done with a modified version of the StarCrash smoothed particle hydrodynamics (SPH) code, available at http://www.astro.northwestern.edu/

StarCrash/. Several previous versions of this code have been used to study a wide range of hydrodynamic interactions between stars (see, e.g., Rasio and Shapiro, 1992; Faber and Rasio, 2000; Sills et al., 2001). SPH is a Lagrangian method which treats the dynamical evolution of a set of finite-sized fluid particles. The density of the fluid is computed at the position of each particle using an interpolation kernel with compact support, extending over a characteristic "smoothing length." In our implementation, the smoothing length around each particle varies in time so as to provide overlap with a nearly constant number of neighboring particles. Hydrodynamic forces are computed using SPH summation techniques (for a detailed derivation, see Rasio and Shapiro, 1992), whereas gravitational forces are calculated using a grid-based FFT convolution method. Shock heating is treated by evolving the energy equation with an artificial viscosity prescription from Balsara (1995).

Computing the full hydrodynamic evolution of both the planet and the star would be very challenging but is in fact unnecessary. Indeed, a simple order-of-magnitude estimate shows that the vast majority of the tidal energy extracted from the orbit will be deposited in the planet during the close interaction. Following Fabian et al. (1975), we expect that for the passage of a planet of mass $M_P$ and radius $R_P$ by a star with mass $M_*$ and radius $R_*$ with periastron separation $r_p$, the tidal energy deposited in the planet and in the star are given respectively by

$$\Delta E_p \simeq f_p^2 \frac{G M_*^2 R_P^5}{r_p^6},$$ (6)

$$\Delta E_* \simeq f_*^2 \frac{G M_P^2 R_*^5}{r_p^6}.$$ (7)

The dimensionless factors $f_p$ and $f_*$ depend primarily on the ratio of the dynamical (crossing) time to the internal dynamical time of each object. Therefore they are mainly a function of the mean density of each object, and should have comparable values for the planet and star. As a result, the ratio of energy dissipated in the planet to that dissipated in the star is

$$\frac{\Delta E_P}{\Delta E_*} \simeq \left(\frac{M_*}{M_P}\right)^2 \left(\frac{R_P}{R_*}\right)^5 \sim 10,$$ (8)

for a Jupiter-like giant planet and a solar-type star. A more detailed analysis based on an expansion over adiabatic nonradial oscillation modes (see, e.g., Lee and Ostriker, 1986) yields exactly the same energy ratio dependence on mass for two equal-density objects to lowest order, albeit with a more complicated functional dependence on the periastron separation $r_p$. Noting these results, we follow the full 3-D hydrodynamic and thermodynamic evolution of the planet, but treat the star as a simple point mass, which interacts with the fluid through gravitational forces only. Although our code can handle fluid particles on grazing trajectories, by treating the stellar surface as an absorbing boundary that captures all SPH particles that pass within $R_* = 10 R_p$, such techniques

play no role in the calculations described here. In no run did any SPH particle fall within that boundary. Our implementation of stellar point-masses is similar in many ways to previous Newtonian SPH treatments of tidal interactions between stars and black holes (e.g., Kluzniak and Lee, 1998), but here we can ignore many of the details regarding the effective boundary around the point-mass. Indeed, the matter lost by the planet and accreted onto the star during extremely close passages has a minimal effect on the stellar mass and completely negligible feedback on the evolution of the orbit.

We define our units in terms of the parameters of the planet, setting $G = M_P = R_P = 1$. In terms of the mass and radius of Jupiter ($M_J = 1.9 \times 10^{30}$ g and $R_J = 7.15 \times 10^9$ cm), this yields characteristic time, velocity, energy, and angular momentum scales of

$$t = 1698 \left(\frac{M_P}{M_J}\right)^{-0.5} \left(\frac{R_P}{R_J}\right)^{1.5} \sec = 1,$$ (9)

$$v = 4.21 \times 10^6 \left(\frac{M_P}{M_J}\right)^{0.5} \left(\frac{R_P}{R_J}\right)^{-0.5} \text{cm/s} = 1,$$ (10)

$$E = 3.37 \times 10^{43} \left(\frac{M_P}{M_J}\right)^2 \left(\frac{R_P}{R_J}\right)^{-1} \text{erg} = 1,$$ (11)

$$J = 5.72 \times 10^{46} \left(\frac{M_P}{M_J}\right)^{1.5} \left(\frac{R_P}{R_J}\right)^{0.5} \text{erg s} = 1.$$ (12)

In all our calculations we fix the mass of the star to be $M_* = 1000 M_P = 0.95 (M_P/M_J) M_\odot$. The planet's equation of state (EOS) is approximated by a $\Gamma = 2$ (or equivalently, $n = 1$) polytrope, i.e., the pressure $P = k\rho^2$, where the entropy constant $k$ is initially set to a fixed value throughout. This EOS has been found to approximate very well the bulk properties of Jupiter-like planets, even though it differs from the ideal gas form at low densities (Hubbard, 1975; Dintrans and Ouyed, 2001). In particular, it provides a mass-radius relation such that radius is independent of mass, agreeing well with detailed models (see Burrows et al., 2003, 2004, and references therein). We note that should the radius of an extrasolar planet be larger, as is predicted for giant planets during early stages of their evolution (see, e.g., Saumon et al., 1996), our results would have to be scaled accordingly.

To model the planet in our calculations, we place SPH particles of varying mass in an equally-spaced hexagonal close-packed lattice, with particle masses set proportional to the polytropic model's density at the appropriate radius. In all calculations shown here, $N = 48846$ particles are used to describe the planet. This number which yields a characteristic smoothing length $h/R_P = 0.05$, has been found in previous calculations to yield results which typically conserve overall energy terms to within $\sim 1\%$ (Faber and Rasio, 2002). The planetary mass distribution is relaxed for 30 dynamical times to achieve a stable configuration, and placed into a very high-eccentricity elliptical orbit around the "point-mass" star at an initial separation $a_0 = 200$. This is sufficiently distant that the initial tidal perturbation of the

planet is negligible. All initial orbits have apastron separations of $r_a = 10^4$, equivalent to 4.78 AU for the parameters of Jupiter. The periastron separation is varied to span a range of values $15 \leqslant r_p \leqslant 50$. For all runs, the planet is initially non-spinning in the inertial frame, with the velocities of all particles set equal to that of the planet's center of mass.

## 3. Calculations and results

The evolution of planets on nearly parabolic orbits is found to be critically dependent on whether or not the orbital separation passes within the Roche limit. We note that although some of the assumptions used to define the Roche limit do not apply to the situation we consider here, the use of the term is still appropriate. Specifically, the Roche limit problem assumes that both bodies are point-masses, and that they both corotate at an orbital velocity corresponding to a circular orbit. Here, the planet is an extended object, it is irrotational in the inertial frame, and the angular velocity during the encounter corresponds to a highly elliptical orbit. Still, the crucial functional dependence on the physical parameters of the system remain exactly the same. We will show with our calculations that the critical separation for the planet to undergo mass loss corresponds extremely closely with the classically defined Roche limit, and thus refer to what is formally the dynamical tidal mass-shedding limit as the Roche limit.

As we demonstrate in Appendix A, the classical Roche limit formulae found in Paczyński (1971) and Eggleton (1983), which treat both components in the system as point masses, underestimate the tidal limit separation (the point at which Roche lobe overflow begins) for our extended, corotating polytropic planetary models placed on circular orbits, by no more than 2%. Indeed, where Paczyński (1971) finds the critical separation for Roche lobe overflow to begin at a separation $a_R = 21.64$, we find that it occurs at a separation that falls somewhere in the range $a_R = 21.8$–22.0.

Our dynamical calculations indicate that for highly elliptical planetary orbits with periastron separations within this limit, mass will be stripped from the planet, where we note that here the planet is assumed to be irrotational in the inertial frame. Funneling out through both the inner and outer Lagrange points in two streams, this mass loss has a significant impact on the future evolution of the planet as well as the orbit, since it can dramatically affect the overall energy and angular momentum budget of the system. Orbits with periastron separations outside the Roche limit still induce energy and angular momentum transfer, but no mass is exchanged between the planet and the star, as we describe in detail below.

### 3.1. Outside the Roche limit

For all systems with initial periastron separations $r_p \geqslant 22$, the passage of the planet by the star resulted in a qualita-
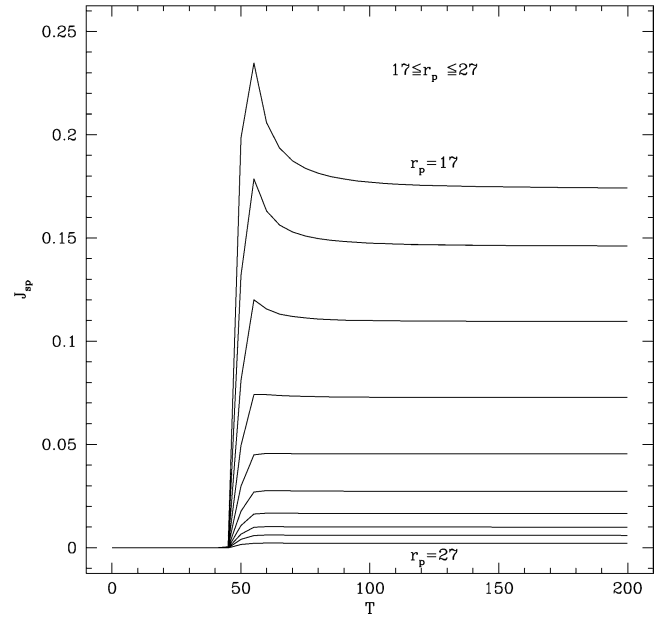


Fig. 2. The evolution of the spin angular momentum over time for all runs shown in Table 1 with periastron separations $17 \leqslant r_p \leqslant 27$. In all cases, we see a spike during the periastron passage, which lasts from $T = 45$–50, before a slight decrease toward the final relaxed value. For the periastron separations shown here, there is a monotonic increase in the final value of $J_{\mathrm{sp}}$ with decreasing $r_p$.

tively similar pattern of tidal energy and angular momentum transfer. The temporal behavior of angular momentum and energy transfer is demonstrated in Figs. 2 and 3, for a number of passages with varying values of $r_p$, and conforms well with the commonly accepted picture of the tidal interaction process. In all cases, we see that energy is transferred into the orbit prior to the periastron passage (which occurs for all models at $T \simeq 45$), without a noticeable change in the angular momentum of the planet. Immediately after periastron, energy is rapidly transferred via tidal effects into the planet, with the tidal torque causing a sharp drop in the total orbital energy. After the passage, the planet gradually relaxes toward a new equilibrium spinning configuration.

It should come as no surprise that for the passages outside the Roche limit in Fig. 3, decreasing the periastron separation leads to both a decrease in the final orbital energy and an increase in the spin angular momentum, since the tidal interaction is much stronger at closer range. These results cannot be generalized to the case of orbits passing within the Roche limit, however, since the final angular momentum and energy distributions are extremely sensitive to the mass loss that occurs in those cases.

As we expect from simple virial arguments, the tidal heating results in some degree of expansion, and a less bound structure for the planet, as shown in Fig. 4. This relationship holds for the entire sequence of orbits we calculated, including those which passed within the Roche limit, as we discuss in more detail below. For passages outside the Roche limit, the amount of energy injected into the planet was not at a sufficient level to unbind any mass from it, down to our reso-
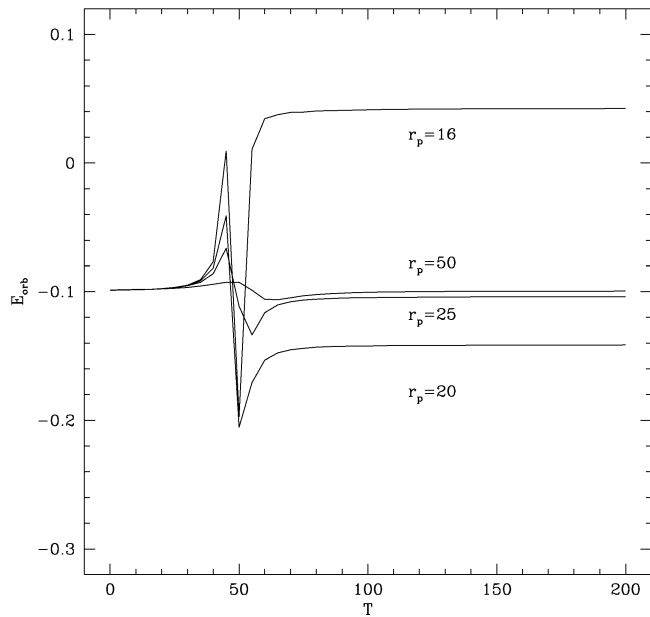
Fig. 3. The evolution of the orbital energy over time for runs with $r_p = 16$, 20, 25, and 50. In all cases, we see energy is injected into the orbit during the first half of the encounter, followed by a rapid decrease of greater magnitude during the second half of the encounter, and finally a long period where the total energy levels off. For the runs with $r_p \geqslant 17.5$, the net energy change is negative, and the final orbit is more bound than the initial one. For $r_p = 16$, we see that the energy required to strip mass from the planet leads to the orbit gaining enough energy to unbind completely.



Fig. 4. The final gravitational binding energy $W$ (solid line), internal thermodynamic energy $U$ (dash-dotted line), and spin kinetic energy $E_{sp}$ (dotted line) of the planet, as a function of periastron separation. Also shown is the virial energy $E_{vir} = W + 3U + 2E_{sp}$, as a dashed line. We see that in all cases the final planetary configuration is nearly virialized. As the total energy for all configurations shown here is negative, we conclude that no Jupiter-like planet can be fully disrupted by a non-grazing passage past a sunlike star.

lution limit (defined by the least massive SPH particles used near the surface of the planet, $m_{min} = 1.5 \times 10^{-7}$). As the periastron separation decreases toward the Roche limit, the energy gained by the planet does increase, causing the planet's radius to increase in corresponding fashion. The various energies and angular momenta describing the final planetary configurations for all the cases we investigated are listed in Table 1. For orbits with $r_p \geqslant 15$ our runs are terminated at $T = 200$, since in all of those calculations the planet had reached a relaxed, virialized configuration by that point. For models with smaller periastron separations, we double the duration of the calculations, letting them run until $T = 400$.

Much of the previous work on tidal capture has used a linear perturbation formalism, developed by (Press and Teukolsky, 1977; see also Lee and Ostriker, 1986), which treats the fluid response to the tidal interaction as a superposition of non-radial adiabatic oscillations. In Appendix B, we summarize the equations describing the energy loss to tidal perturbations, and give the coefficients in the expansion for configurations with EOS appropriate for both a gas giant ($\Gamma = 2$) and, for completeness, a terrestrial planet ($\Gamma = 3$) (Boss, 1986). Outside the Roche limit, we find that the Press–Teukolsky formalism gives the proper scalings for the tidal interaction process, but slightly underestimates the overall magnitude of the effect. In Fig. 5, we show the final orbital energy as a function of periastron separation for all the models we computed, as well as the estimate obtained from the linear perturbation analysis. We find that
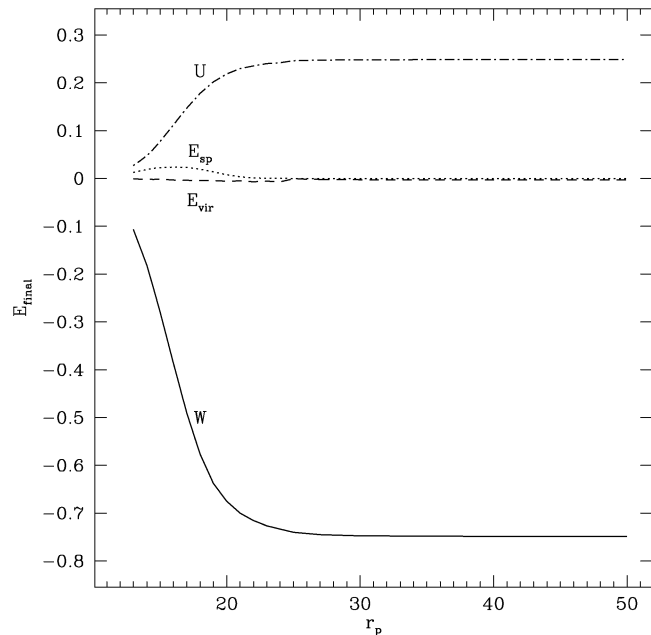
while the power-law scalings are very similar, the perturbation analysis typically yields a change in the orbital energy approximately half the magnitude of what we find from our SPH calculations. The relationship breaks down completely for $r_p < 20$, when the deformation of the planet undergoing mass loss clearly becomes nonlinear. We note that the nearly constant change in orbital energy we find from our calculations at periastron separations $r_p \geqslant 30$ are a numerical artifact, and represent the smallest change in energy we can accurately measure over the full timescale of one of our evolution calculations.

### 3.2. Within the Roche limit

For initial orbits with $r_p \leqslant 21$, the planet passes within the classical Roche limit (for a mass ratio $q = 0.001$, the critical separation for Roche lobe overflow is $a_R = 21.64$, according to Eq. (3)). In all the cases we looked at in this regime, fluid was stripped from the planet, escaping in extremely narrow streams through both the inner (L1) and outer (L2) Lagrange points. We show the evolution of one such system, with $r_p = 18$, in Fig. 6. The axes are defined such that the planet orbits counter-clockwise along an orbit whose unperturbed pericenter would fall on the negative $x$-axis, and the timescale initialized to the initial configuration at separation $a_0 = 200$. In the first panel, we show the configuration of the planet at $T = 45$, shortly before periastron, as well as the star, whose physical size is indicated

Table 1
Run results

| $r_p$ | $\Delta m$ | $\Delta m_{\rm in}$ | $E_{\rm orb}$ | $J_{\rm orb}$ | $r_{\rm max}$ | $E_{\rm sp}$ | $J_{\rm sp}$ | $W$ | $U$ | $R_{95}$ | $R_{100}$ |
|---|---|---|---|---|---|---|---|---|---|---|---|
| 12 | 5.8E−1 | 3.2E−1 | 1.77E−1 | 62 | hyp | 4.68E−3 | 1.26E−1 | −0.052 | 0.014 | 8.77 | 57.2 |
| 12.5 | 5.4E−1 | 3.9E−1 | 6.80E−2 | 70 | hyp | 6.66E−3 | 1.16E−1 | −0.077 | 0.021 | 7.68 | 62.8 |
| 13 | 4.9E−1 | 2.7E−1 | 9.11E−2 | 81 | hyp | 9.94E−3 | 1.45E−1 | −0.103 | 0.027 | 6.75 | 58.2 |
| 13.5 | 4.2E−1 | 2.4E−1 | 1.63E−1 | 93 | hyp | 1.30E−2 | 1.69E−1 | −0.140 | 0.038 | 5.87 | 57.1 |
| 14 | 3.7E−1 | 2.1E−1 | 1.22E−1 | 105 | hyp | 1.53E−2 | 1.77E−1 | −0.177 | 0.049 | 5.35 | 56.3 |
| 14.5 | 3.0E−1 | 1.8E−1 | 1.30E−2 | 117 | hyp | 1.72E−2 | 1.91E−1 | −0.224 | 0.063 | 5.06 | 61.1 |
| 15 | 2.4E−1 | 1.5E−1 | 1.25E−1 | 131 | hyp | 2.27E−2 | 1.98E−1 | −0.279 | 0.077 | 3.58 | 38.8 |
| 16 | 1.5E−1 | 9.3E−2 | 9.37E−3 | 153 | hyp | 2.36E−2 | 1.90E−1 | −0.385 | 0.111 | 2.75 | 36.1 |
| 17 | 7.2E−2 | 5.0E−2 | −5.68E−2 | 171 | 1.63E3 | 2.30E−2 | 1.74E−1 | −0.491 | 0.147 | 1.82 | 37.4 |
| 18 | 2.7E−2 | 2.1E−2 | −1.15E−1 | 184 | 8.42E3 | 1.97E−2 | 1.46E−1 | −0.577 | 0.177 | 1.30 | 37.6 |
| 19 | 6.4E−3 | 5.7E−3 | −1.43E−1 | 193 | 6.95E3 | 1.37E−2 | 1.10E−1 | −0.637 | 0.202 | 1.11 | 38.4 |
| 20 | 5.8E−4 | 5.6E−4 | −1.42E−1 | 200 | 7.04E3 | 7.60E−3 | 7.27E−2 | −0.676 | 0.218 | 1.02 | 38.2 |
| 21 | 1.2E−6 | 3.5E−7 | −1.28E−1 | 205 | 7.82E3 | 3.45E−3 | 4.53E−2 | −0.700 | 0.229 | 0.97 | 33.9 |
| 22 | 0.0 | 0.0 | −1.17E−1 | 209 | 8.49E3 | 1.35E−3 | 2.73E−2 | −0.715 | 0.235 | 0.94 | 1.11 |
| 23 | 0.0 | 0.0 | −1.10E−1 | 214 | 9.06E3 | 5.19E−4 | 1.65E−2 | −0.726 | 0.240 | 0.93 | 1.06 |
| 24 | 0.0 | 0.0 | −1.06E−1 | 219 | 9.40E3 | 1.92E−4 | 9.89E−3 | −0.733 | 0.242 | 0.92 | 1.03 |
| 25 | 0.0 | 0.0 | −1.04E−1 | 223 | 9.60E3 | 7.71E−5 | 5.90E−3 | −0.740 | 0.246 | 0.91 | 1.03 |
| 27 | 0.0 | 0.0 | −1.01E−1 | 232 | 9.89E3 | 1.48E−5 | 2.03E−3 | −0.745 | 0.248 | 0.90 | 1.00 |
| 30 | 0.0 | 0.0 | −9.97E−2 | 244 | 1.00E4 | 1.85E−6 | 4.44E−4 | −0.747 | 0.248 | 0.89 | 0.98 |
| 40 | 0.0 | 0.0 | −9.95E−2 | 282 | 1.00E4 | < 1E−6 | < 1E−4 | −0.749 | 0.249 | 0.89 | 0.97 |
| 50 | 0.0 | 0.0 | −9.95E−2 | 315 | 1.00E4 | < 1E−6 | < 1E−4 | −0.749 | 0.249 | 0.89 | 0.97 |

*Note.* Results of our runs. Here $r_p$ is the initial periastron separation, $\Delta m$ the mass unbound from the planet, $\Delta m_{\rm in}$ the amount of mass lost from the planet but bound to the star, $E_{\rm orb}$ and $J_{\rm orb}$ the final orbital energy and angular momentum, $r_{\rm max}$ is the new value of the apastron separation after the encounter for systems which remain bound ("hyp" indicates the planet leaves on a hyperbolic orbit), $E_{\rm sp}$ and $J_{\rm sp}$ the final spin energy and angular momentum of the planet, $W$ and $U$ the planet's gravitational binding and internal heat energies, and $R_{95}$ and $R_{100}$ are the radius of the final bound configuration containing 95% and all of the bound matter, respectively, with initial values of 0.89 and 1.00. All energy and angular momenta quantities are overall totals, not specific totals with the mass dependence divided out. Units are defined such that $G = M_P = R_P = 1$.

by the large circle. The planet is beginning to show signs of tidal deformation (looking roughly ellipsoidal). Note again that the stellar size is merely illustrative, and plays no role in the calculations, since no matter from the planet crosses within the stellar radius during our calculation. In the second panel, at $T = 50$, immediately after periastron passage, we see the planet starting to distend further, as matter crosses through the Lagrange points while tidal energy is transferred into the planet. At $T = 75$, two mass-shedding streams are clearly evident. We find that all particles in the inner stream, representing a total mass $\Delta m_{\rm in} = 0.021$ are no longer bound to the planet, but remain gravitationally bound to the star. By contrast, particles in the outer stream, representing a total mass $\Delta m_{\rm out} = 5.9 \times 10^{-3}$, are bound to neither the star nor the planet, and will be ejected from the system. In the final frame, we find at $T = 150$ that fluid in both streams has assumed an essentially ballistic trajectory, freely falling in the star's potential well. Particles from the inner stream trace out nearly elliptical orbits, retaining enough angular momentum to pass outside the star's surface, while those in the outer stream head away from the system on hyperbolic orbits, leading the path of the planet in an almost cometary fashion.

We can make a few general statements with regard to orbits within the mass-shedding regime. First, in all cases we investigated, the amount of mass stripped from the planet increased with decreasing periastron separation, as shown in Fig. 7. The rise seems to be almost exponential near the

Roche limit, but flattens out at smaller values, such that even for orbits on which the planet will graze the edge of the star during the passage, it will *not* be completely unbound by the interaction. This is in agreement with previous results for tidal disruptions of stars around massive black holes (Luminet and Carter, 1986; Evans and Kochanek, 1989), that indicate full disruption only occurs for stars on orbits with periastron separations meeting the criterion $\eta \lesssim 1.0$, where the interaction strength $\eta$ is defined by the relation

$$\eta \equiv \left( \frac{M_2}{M_1 + M_2} \right)^{0.5} \left( \frac{r_p}{R_2} \right)^{1.5}, \tag{13}$$

where $M_1$ and $M_2$ are the masses of the more massive object and the body being disrupted, respectively (here, $M_1 \equiv M_*$ and $M_2 \equiv M_P$). For systems with $q \ll 1$ and equal-density components, this condition essentially yields $r_p < R_*$. In other words, planets would to have to pass within the star in order to be fully disrupted.

In all cases we studied (except the orbit with $r_p = 21$, in which fewer than 10 SPH particles became unbound), the amount of matter stripped from the planet along the inner stream, which remains bound to the star, exceeds the amount of matter unbound from the system through the outer stream. This asymmetry in the mass of the two tidal streams is greatest near the Roche limit. Indeed, for orbits with $18 \leqslant r_p \leqslant 20$, we find that over 75% of the mass stripped from the planet can be found in the inner stream. For orbits with smaller periastron separations, especially those nearing the limit of a grazing collision, the mass ratio in the two
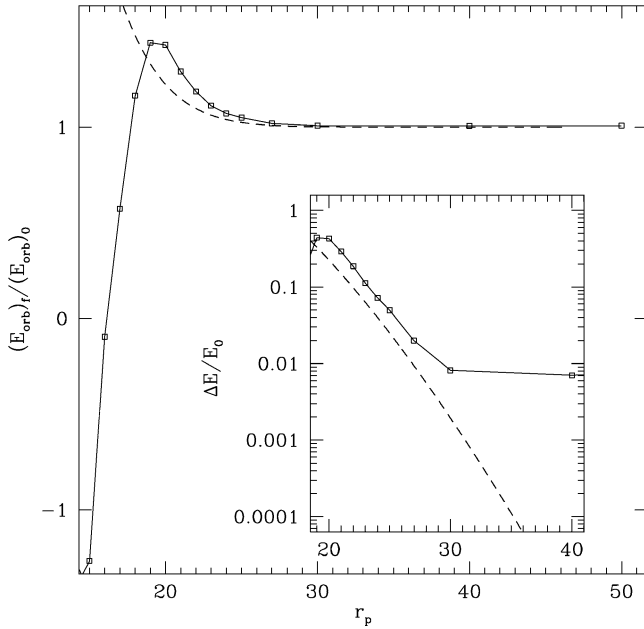
Fig. 5. The relative change in the orbital energy from the beginning of our calculations to the end, as a function of the periastron separation (solid curve). We see that this quantity increases as we sweep inward (becoming more negative), indicating more tightly bound orbits, until reaching a maximum at $r_p \approx 19.5$. Within this periastron separation, systems become successively less bound (the orbital energy less negative), until at $r_p \approx 16.2$ we find that the planet becomes unbound from the star and leaves on a hyperbolic trajectory. The dashed curve shows the predicted behavior from a Press–Teukolsky type analysis of non-radial adiabatic oscillations as described in Appendix B. This approximation scales well at large separations, up to $r_p \sim 30$ where the systematic errors in the total energy become larger than the net change, and breaks down for $r_p < 20$ when the linear regime itself is no longer applicable.



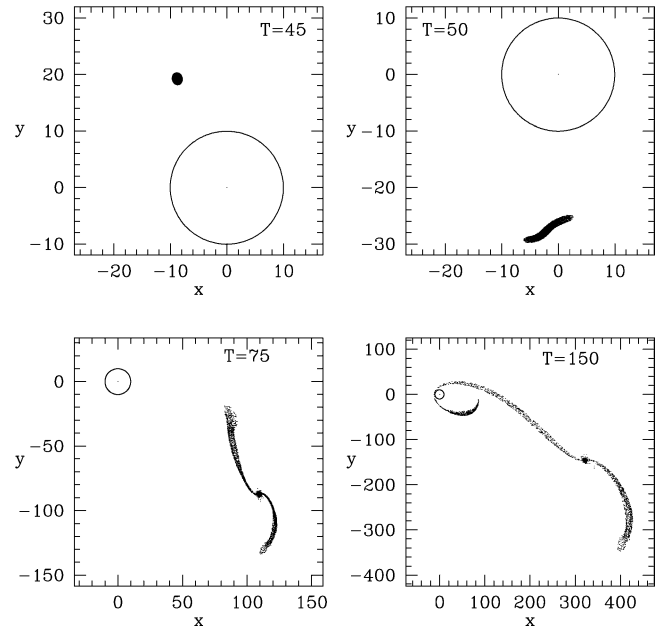Fig. 6. Evolution of the planet along an orbit with periastron separation $r_p = 18$. In the upper left panel, we see the planet, orbiting counter-clockwise, nearing periastron at $T = 45$ past the star, whose physical radius is indicated by the circle. In the upper-right, at $T = 50$, we see the planet immediately after periastron, with strong tidal effects obvious. In the lower left, we see at $T = 75$ that a pair of mass-shedding streams have formed, both toward the star and away. Eventually, by $T = 150$, we see the inner stream has stretched all the way around the star, as the particles follow essentially free-fall trajectories in the star's gravitational well. Note the different size scales for each plot. For clarity, only particles near the orbital plane are shown.

streams nears unity. While at first glance these results may appear to differ slightly from the picture developed for the disruption of a star by a massive black hole in Lacy et al. (1982), Rees (1988), and Evans and Kochanek (1989), we note that their calculations were performed for orbits with $\eta \sim 1.0$, which represents a periastron separation here of $r_p = 10.0$. Summarized, when the tidal energy $\Delta E$ injected into the smaller body is greater in magnitude than the binding energy $E_B$ of the object, we expect it to be disrupted. The velocities of fluid elements in the smaller object take on a range of values, depending on the depth of the passage through the potential well, with a roughly flat distribution of specific energies centered near zero, since $\Delta E \gg E_B$ (see Fig. 3 in Evans and Kochanek, 1989). The fluid with negative specific energy becomes bound to the larger body in the system, and that with positive specific energy unbound, representing nearly equal amounts. For the planet–star interactions we investigate here, we expect to find equal masses deposited into the inner and outer streams only in the limit of grazing collisions, for which $\Delta E \sim E_B$. Such a conclusion cannot be generalized to passages with larger values of $r_p$ since the magnitude of the tidal bulge does not approach the same scale as the planet's radius, or in other terms, the tidal energy remains smaller than the overall self-binding
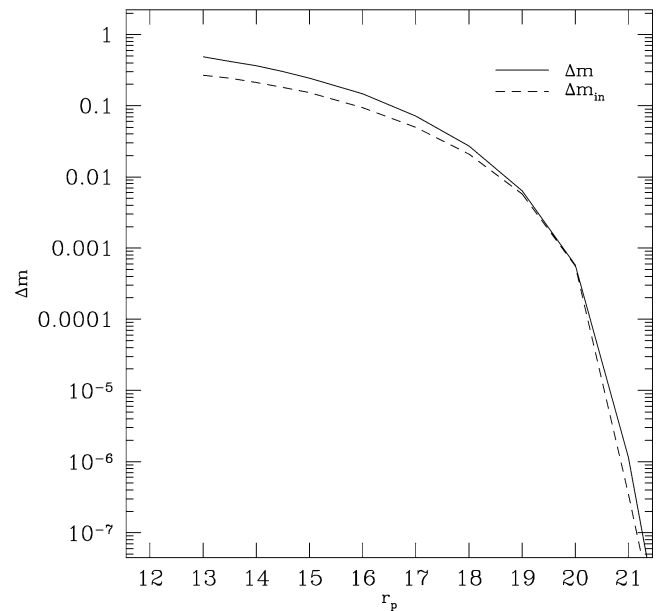


Fig. 7. The total mass unbound from the planet during the interaction (solid line) and the mass which ends up bound to the star (dashed line), as a function of periastron separation. As a rule, matter in the inner mass shedding stream ends up bound to the star, whereas matter in the less massive outer stream is completely unbound.

energy of the planet. Furthermore, in terms of the interaction strength $\eta$, we expect that disruption of a Jupiter-like planet by a solar-type star should require a tighter passage than for a solar-type star being disrupted by a massive black hole of $M_{BH} \approx 10^6 M_\odot$. Indeed, the characteristic expansion velocity $v_{exp}$ of the secondary as it is being disrupted scales like $v_{exp} = (M_1/M_2)^{1/6} v_{esc}$, where $v_{esc}$ is the escape velocity from the its surface. Thus, the characteristic expansion velocity within a star being disrupted by a massive black hole ($M_1/M_2 = 10^6$) is more than double that for a planet being disrupted by a star ($M_1/M_2 = 10^3$), relative to the respective escape velocities. We conclude that the core of the planet should remain bound for passages with lower values of $\eta$ than for the stellar-massive black hole case.

For close passages, the planet experiences a radial expansion, due to strong tidal heating throughout. As the periastron separation decreases, $R_{95}$, defined as the radius enclosing 95% of the planet's bound mass at the end of the calculation, increases to a value a few times larger than that of the planet prior to the encounter, especially in cases with $r_p \lesssim 18$. For all mass-shedding systems, the furthest gravitationally bound particles, at a distance $R_{100}$ from the planet's center of mass, were found to be located at $R_{100} > 30$. This state would almost certainly not be permanent, and merely reflects the extremely long dynamical relaxation timescale found in the low-density outer regions of the planet. Since the dynamical timescale has a power-law dependence proportional to $\rho^{-0.5}$, the matter furthest from the planet (and thus with the lowest density) requires considerably more time than we can feasibly calculate to reach equilibrium. However, since this represents an extremely small fraction of the total mass, we do not expect the long-term relaxation of the planet's outer regions to affect our results about the dependence of various energy quantities on the periastron separation.

Several quantities we tabulate do not show monotonic dependence on the periastron separation of the planet's orbit. We see in Fig. 5 that it is only for the range $r_p \geqslant 19.5$ that the final orbital energy becomes more strongly negative as the periastron separation decreases. For these cases, the apastron separation of the post-encounter orbit decreases with decreasing $r_p$ (the periastron separation, as one should expect, remains essentially fixed after the encounter, since the specific orbital angular momentum changes very little during the encounter). Indeed, the orbital energy reaches an extremum and begins to become less negative (the orbit less tightly bound) as $r_p$ decreases below the critical value $r_p = 19.5$. For orbits with $r_p < 17.5$, there is a net *gain* in the orbital energy of the planet. For periastron separations $r_p \lesssim 16.2$, the orbital energy becomes positive, and the planet leaves the system on an unbound hyperbolic trajectory. This can also be seen in Fig. 3, as the run with $r_p = 16$ demonstrates a characteristically different pattern than those at larger separations. The tidal interaction leads to a sharp increase in the orbital energy followed immediately by larger decrease. This is followed by significant mass loss
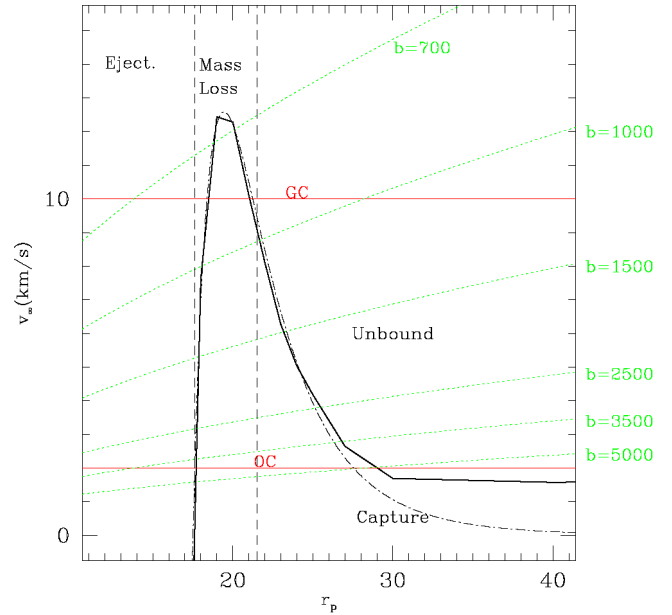


Fig. 8. The critical value $v_{capt}$ of the relative velocity at large distances, $v_\infty$, for which a planet can be captured, as a function of the periastron separation (solid line). Velocities below the curve lead to capture, those above the curve to unbound systems. For $r_p \lesssim 17.5$, there is a net gain in orbital energy, and no bound system can be formed. Also shown are curves of constant initial impact parameter $b$, as well as the typical relative velocities within a globular cluster ($v_\infty = 10$ km/s) and an open cluster ($v_\infty = 2$ km/s). The dot-dashed line shows the approximate fit, Eq. (16), which we use to estimate the capture timescale.

from the planet, leaving only $\sim 40\%$ of the original mass of the planet gravitationally bound. A great deal of material which once formed the planet becomes bound to the star instead, causing a strong *increase* in the orbital energy of the surviving planet. A similar pattern was seen for all passages with $r_p \leqslant 16$.

We can use these results to classify the fate of planets passing by stars on either bound or unbound orbits. In Fig. 8, we show the critical relative velocity at large separations leading to capture, $v_{capt} \equiv \sqrt{2(\Delta E_{orb})/\mu}$, as a function of $r_p$. Here $\mu \approx M_P$ is the reduced mass of the system. If the relative velocity of the star and planet at large separations falls below the critical value, the planet can be tidally captured during the interaction. Note that these results may underestimate the true capture velocity by $\sim 5\%$, since we have ignored tidal dissipation in the star. Of course, since the energy loss scales $\propto r_p^{-6}$, this represents less than a 2% correction to the maximum capture radius for a given relative velocity. We see that in a globular cluster, where the typical relative velocity is $\sim 10$ km/s, there is a very low probability of forming bound systems through tidal capture. For an open cluster, however, with a typical velocity dispersion of 2 km/s, close passages satisfying $18 \lesssim r_p \lesssim 30$ are likely to meet this criterion. At the high end, our main source of uncertainty is a systematic overestimate of $v_{capt}$, since deviations from equilibrium in our initial conditions act as a small spurious energy source for the orbit. To con-

firm our estimate of the maximum capture velocity at large separations, we computed additional runs with periastron separations of $r_p = 40$ and $r_p = 50$, for orbits with zero total energy (parabolic), and small positive energies (hyperbolic with $v_\infty = 0.05 = 2$ km/s and $0.1 = 4$ km/s). As expected, we find that the total change in the orbital energy is essentially unchanged, since the interaction timescale is set by the orbital velocity at periastron, which depends very strongly on the periastron separation but extremely weakly on the total orbital energy.

To calculate cross sections for these collisions, the important quantity is the impact parameter of the hyperbolic orbit,

$$b = r_p \sqrt{1 + \frac{2GM_*}{r_p v_\infty^2}}, \qquad (14)$$

rather than the periastron distance. To give some sense of the size scales involved, for a globular cluster with $v_\infty = 10$ km/s, the narrow typical range of capturable periastron separations, $18.5 < r_p < 21$, yields a correspondingly narrow range of impact parameters, $770 < b < 820$. For an open cluster with $v_\infty = 2.0$ km/s, the range of periastron separations $18 < r_p < 30$ corresponds to a wider range of impact parameters for capture, $4000 < b < 5000$, or roughly $2.0$ AU $< b < 2.4$ AU.

It is relatively straightforward to expand this analysis toward a more physically realistic picture of tidal capture. Following Gaudi (2003), we will assume that planets and stars move within some form of cluster (either globular or open) with the same characteristic velocity dispersion $\sigma$. Such a condition would theoretically result after planets are liberated from their original parent stars by a series of weak encounters, but before thermal relaxation causes them to gain sufficient velocity to escape the cluster. Furthermore, we will assume that the number density of stars $\nu$ is uniform, to simplify the calculation. Following the logic of Section 8.4.5 of Binney and Tremaine (1987), we find that the average collision time $t_c$ required for a planet to pass within a distance $r_p$ from a star is given by

$$t_c^{-1} = \frac{\nu\sqrt{\pi}}{2\sigma^3} \int\limits_0^\infty e^{-v_\infty^2/4\sigma^2} \left(v_\infty^3 r_p^2 + 2GM v_\infty r_p\right) dv_\infty. \qquad (15)$$

Note that the latter term in parentheses above, representing gravitational focusing, differs from that presented in Eq. (8-121) of Binney and Tremaine (1987), since they are discussing the case of equal-mass stars, for which $M = 2M_*$. Here, for planet–star encounters, $M \simeq M_*$. As we have seen in Fig. 8, the condition for tidal capture is more complicated than simply having the periastron fall within a certain limit, since sufficient energy needs to be dissipated to create a bound orbit. Instead, for a given value of $v_\infty$, the periastron separation must lie within a range of values $r_1(v_\infty) \leqslant r_p \leqslant r_2(v_\infty)$. We find that $r_1$ and $r_2$ can be determined implicitly, to more than sufficient accuracy, as roots of the relation

$$v_\infty = 5 \times 10^3 \frac{r - 17.5}{(r/10.0)^{10}} \text{ km/s}, \qquad (16)$$

which is shown as a dot-dashed line on Fig. 8. We integrate Eq. (15) only up to the maximum possible capture velocity, and only for ranges of periastron separations $r_1 < r_p < r_2$, for the three cases considered by Gaudi (2003): a globular cluster ($\sigma = 10$ km/s, $\nu = 10^4$ pc$^{-3}$), a rich open cluster ($\sigma = 1.5$ km/s, $\nu = 10^3$ pc$^{-3}$), and a loose stellar association ($\sigma = 0.6$ km/s, $\nu = 10^2$ pc$^{-3}$). In all cases, it is the gravitational focusing term which dominates, since $GM_*/r_p \gg v_{\text{capt}}^2$ for each. We find capture timescales, respectively, of $2.1 \times 10^4$ Gyr (globular cluster), $4.5 \times 10^3$ Gyr (open cluster), and $1.3 \times 10^4$ Gyr (loose association). The systematic error in estimating $v_{\text{capt}}$ for large values of $r_p$, discussed above, plays essentially no role in our final results for the globular cluster, and introduces an uncertainty of approximately 2 and 10% in the rate for open clusters and loose associations, respectively. Gaudi (2003) overestimates the capture rate, due to a numerical error in the capture timescale formula (Eq. (7); the denominator should have a 2, not an 8), and by assuming capture for closer passages in which mass is lost but the planet remains on a hyperbolic orbit.

Regardless of whether the planet's initial orbit is hyperbolic or elliptical, we expect that several distinct phenomena should occur for passages with sufficiently small periastron separations. For $r_p \lesssim 21$, we expect that some amount of mass loss will occur, regardless of whether the system ends up bound or unbound. For all systems with $r_p \lesssim 17.5$, we expect that no tidal capture can occur, since there is a net gain in orbital energy. In addition, we expect significant mass loss ($\Delta M > 0.25M$) for systems with $r_p \lesssim 15$.

The final orbital parameters for our runs are given in Table 1. Note that mass contained in the inner stream, $\Delta m_{\text{in}}$, is treated here as if it will eventually accrete onto the star when we determine the orbit. While this may not hold in detail for all matter in the stream (since some small fraction of the matter may be heated or shocked and attain enough energy to be ejected form the system), its mass as a fraction of the star's total mass is virtually negligible. To compute the orbital energy and angular momentum, we include both the point-mass star and all particles bound to it when calculating its center-of-mass, and only those particles bound to the star when calculating its position. These results are only intended to describe the binary configuration present at the end of the dynamical encounter. Thermal and radiative processes will certainly affect the structure of the planet, and additional mass loss may occur, changing the orbital parameters (Guillot and Showman, 2002). Such phenomena cannot be properly described by an SPH treatment, however.

## 4. Conclusions

Based on recent observations of three extrasolar planets with orbital periods of < 2 days but radii comparable to that of Jupiter, we suggest that these planets may have either been scattered onto very highly eccentric orbits through dynam-

ical interactions in their protoplanetary systems or tidally captured from free-floating trajectories. Through a series of tidal encounters at periastron, energy can be dissipated until the orbit eventually reaches the ideal circularization radius, at a distance almost exactly twice that of the Roche limit.

Numerical calculations confirm that the classical Roche limit plays an important role in these interactions, since it sets the boundary that determines whether or not mass will be stripped from the planet during periastron passage. In turn, mass loss can play a significant role in the resulting energy and angular momentum budgets, with regard to both the orbital and spin evolution of the planet.

For orbits with periastron separations that lie outside of the Roche limit, we find that a Press–Teukolsky expansion over linear, non-radial, adiabatic oscillations provides a good estimate of the energy and angular momentum transfer between the orbit and the planet. For closer passages, however, the linear formalism breaks down, as mass is stripped off the planet through both the inner (L1) and outer (L2) Lagrange points. Still, we find that the planet will never be fully disrupted on any orbit that does not result in a collision with the star. Because the stripped mass acts as an energy sink, we find that the maximum negative change in orbital energy for the planet occurs for encounters just within the Roche limit. For smaller separations, $r_p \lesssim 19$, the energy loss from the orbit decreases, since a greater fraction of the tidal energy is used to unbind mass from the planet. For periastron separations $r_p \lesssim 17.5$, the net change in orbital energy turns positive, and the planet, with smaller mass after the encounter, is ejected from the system on a hyperbolic orbit.

Our results can be extended to predict the fate of earth-like planets undergoing strong tidal encounters as well. For the Earth–Sun system, the Roche limit is reached at a periastron separation of $r_p = 1.38 R_\odot$. Strong tidal encounters, defined as those with interaction strength $\eta = 1$, only occur for passages with $r_p \leqslant 0.64 R_\odot$, leading us to conclude that terrestrial planets would have to pass well within the star in order to be tidally disrupted.

The biggest problem for models which invoke long term tidal circularization of orbits involves dissipating the energy injected into the planet while the orbit circularizes. Several planetary evolution calculations have predicted that planets on elliptical orbits with periods $P \lesssim 3$ days should expand to the point where they fill their Roche lobe, and begin to transfer mass to the parent star, eventually leading to disruption of the planet (Gu et al., 2003, 2004). If this is true, however, it is unclear how one can explain the past orbital evolution of OGLE-TR-56b and the other systems whose orbital periods fall within this limit, on what are now circular orbits. One of two possible explanations seems to be required to explain the data we confront today. First, if planets are unable to survive the expansion resulting from tidal heating during orbital circularization, we need to determine a mechanism whereby planets migrate inward, perhaps during the evolution of the protoplanetary disk, but stop at *twice the Roche*

*limit*. The answer seems not to lie in Roche lobe overflow for this case, since recent observations (Torres et al., 2004) and theoretical calculations (Burrows et al., 2004) indicate that OGLE-TR-56b has a radius of $1.23 \pm 0.16 R_\odot$, which is well within the Roche lobe. Alternately, as presented here, these planets may undergo tidal encounters with stars after being kicked into highly eccentric orbits or captured from the field, eventually circularizing at a distance equivalent to twice the Roche limit, as the current observed population suggests. If this is true, then some new mechanism must be constructed to explain how such planets radiate away the dissipated energy before they are disrupted. At the moment, there is no detailed theoretical model which seems to provide the complete picture, but work is underway to model the detailed evolution of rotating planets undergoing a succession of tidal interactions during periastron passages (see, e.g., Ivanov and Papaloizou, 2004b).

Since the change in orbital energy for the interactions we investigated here is significantly larger than the total energy of the systems, we conclude that our results should hold equally true for nearly parabolic orbits with slightly positive total energy, i.e., tidal captures of planets on weakly hyperbolic orbits with small relative velocity $v_\infty$. The parameter space for encounters that lead to capture into a bound orbit is limited, however, primarily because of the mass-stripping effect. Essentially, if a planet passes too far from the star, it will not be captured, but if it passes too close, so much energy is used to unbind its outer layers that the planet is boosted to an even higher energy hyperbolic orbit. The parameter space of orbits leading to tidal capture is significantly greater for open clusters, with a typical velocity dispersion of $\sim 2$ km/s, than for globular clusters ($\sim 10$ km/s) but the dramatically lower spatial density of planets and stars is likely to hinder the capture process. Still, based on approximate parameters for these systems, although we expect that the capture timescale for planets will be almost 5 times shorter in open clusters, the significantly greater number of stars in globular clusters should lead to a higher overall capture rate.

Our detailed calculations suggest that the results of Gaudi (2003) may need to be recalculated, since his assumptions about the fate of planets after tidal interactions uses an overly simplistic dependence on the periastron separation. In that paper, he argues that according to simple analytic approximations, a planet with mass $M_P = 0.001 M_*$ must pass within two stellar radii ($r_p \lesssim 20 R_P$ for our chosen parameters) in order to be captured. We find that this upper limit should be placed further out, but with a non-trivial dependence between the initial relative velocity of the planet and star and the critical periastron separation for capture. We also find that a lower limit can be placed on capturable orbits from the condition that the net change in orbital energy must be negative, which only occurs for orbits with $r_p \gtrsim 17.5$. By adding these considerations to a proper long-term treatment of the production and capture of free floating planets in stel-

lar clusters we may be able to pin down more accurately the true capture rate and properties of the resultant systems.

## Acknowledgment

## Appendix A. The Roche limit

Even though the duration of the close passage of a gas giant past a star on an elliptical quasiparabolic orbit is extremely short in comparison to the orbital period, it is relatively long compared to the internal hydrodynamical timescale of the planet. Thus, one might possibly guess that if the planet passes within the classical Roche limit, it should lose mass, whereas those that pass outside the Roche limit will not. As we will demonstrate below, this simple guess is manifestly correct, even though the situation we consider is posed somewhat differently than the classic Roche problem.

Our dynamical models violate three assumptions that underlie the Roche lobe calculations. First, planets are extended objects, whereas the Roche lobe approximation is solved for the gravitational potential field around a pair of point masses. Second, the planets in our calculation are irrotational in the inertial frame, rather than synchronized. Third, the orbital velocity at periastron passage is $\sqrt{2}$ times as large for a nearly parabolic orbit as it is for a circular orbit, so the angular velocity of the corotating frames are different.

It is relatively easy to test out the effects of the first of these simplifications using SPH techniques. Since the material in a synchronized planet on a circular orbit is stationary in the corotating frame, we can use relaxation techniques to construct equilibrium configurations for a given orbital separation. First, to account for the rotating frame, we add to the force equation a centrifugal acceleration term $\vec{a}_{cent} = \Omega^2 \vec{r}$, where the angular velocity $\Omega$ is calculated at every timestep so that the outwardly directed centrifugal force exactly balances the inward gravitational force on each member of the system. To drive the system toward equilibrium, we also add a velocity damping term, $\vec{a}_{damp} = -\vec{v}/t_{relax}$, where we set $t_{relax} = 1$. The planet is initially laid down in a spherical configuration, with an initial orbital separation $a_0 = 25$, slightly outside the Roche limit, $a_R = 21.64$, which we find for $q = 0.001$ from Paczyński (1971). The planet is allowed to evolve for 25 dynamical times toward the proper tidally extended equilibrium state while the orbital separation is kept fixed. Next, we slowly decrease the orbital separation, sufficiently slowly that the planet can remain in quasi-equilibrium during the process. Eventually, the planet fills its Roche lobe and matter crosses through the inner Lagrange point toward the star. As shown in Fig. 9, we find that this happens at a separation $a \approx 22.0$, as depicted in the
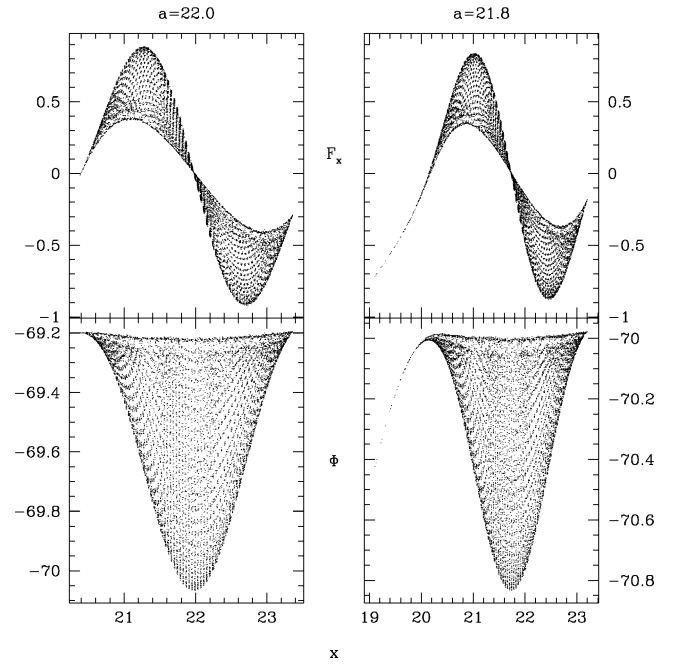


Fig. 9. Gravitational force $F_x$ along the orbital axis (top panels) and gravitational potential $\Phi$ (bottom panels) for synchronized quasi-equilibrium configurations just outside the Roche limit at separation $a = 22.0$ (left panels) and just within the Roche limit at separation $a = 21.8$ (right panels). For clarity, only particles near the equatorial plane, with $|z| < 0.05$ are shown. Our estimate of the Roche limit agrees extremely well with that from Paczyński (1971).

left hand panels. In the top plot, we show the gravitational force in the rotating frame in the $x$-direction (the direction of the orbital separation vector) as a function of position for all particles near the orbital plane satisfying $|z| < 0.1$. We see that particles on the innermost edge of the planet experience almost no net gravitational force, indicating that they are extremely close to the inner Lagrange point. The bottom panel, showing the gravitational potential for these same particles, with the centrifugal barrier terms factored in, yields the same conclusion. In the right hand panels, we show the same quantities when the orbital separation has been reduced to $a = 21.8$, showing clear evidence that the innermost particles making up the planet have crossed through the inner Lagrange point and are now bound to the star instead.

Thus, we see that even though the exact conditions used to determine the Roche limit do not apply in detail to extended polytropic configurations, the simplest approximation formulae for the Roche lobe radius as a function of the system mass ratio (Paczyński, 1971; Eggleton, 1983) are still accurate to within approximately 2%. While the assumptions underlying the classical Roche limit, i.e., synchronized spins and the angular velocity corresponding to a circular orbit, are violated by irrotational planets on quasiparabolic orbits, we find that the critical point at which mass is stripped from the planet does fall very near this line, and in a small abuse of notation we will refer to the latter as the "Roche limit" as well. It should be noted, though, that this latter quantity may

very well have weak but non-trivial dependence on the planet's spin and the orbital parameters.

## Appendix B. Linear, non-radial, adiabatic oscillations

So long as the periastron separation of the orbit is sufficiently large, the perturbations to the planetary structure will remain squarely in the linear regime. Tidal capture through energy losses to adiabatic, non-radial oscillations was studied in detail by Press and Teukolsky (1977), who expanded greatly on the analytical treatment devised by Fabian et al. (1975). This work was extended by Lee and Ostriker (1986), who determined approximate power-law relations which govern the energy transfer scaling at large separations, and corrected an error in the original Press–Teukolsky paper. Their work focused on $n = 3/2$, 2, and 3 polytropes, all of which had adiabatic indexes $\Gamma_1 \equiv d \ln P / d \ln \rho = 5/3$, appropriate for general polytropic stellar models. These results have been used to study a variety of phenomena related to tidal capture, including the tidal damping of oscillations through mode–mode coupling and luminosity variations for radio pulsars in eccentric orbits (see, e.g., Kumar et al., 1995; Kumar and Goodman, 1996).

Here, we extend this method to cases appropriate for the planetary models we calculate. For gas giants, we assume an EOS with $n = 1$, $\Gamma_1 = 2$, and for an earthlike planet, we take $n = 0.5$, $\Gamma_1 = 3.0$. As $n = 1/(\Gamma_1 - 1)$ for these models, we know that we can ignore g-mode oscillations, and are left only with the f-mode and p-mode cases.

To determine the oscillation mode frequencies and overlap integrals, corresponding to Tables 1A and 1B of Lee and Ostriker (1986), we used a code which solves four linked, linearized, first-order equations of adiabatic motion (see, e.g., Ledoux and Walraven, 1958; Dziembowski, 1971), integrating inward from the surface and outward from the center, and matching the solutions at the midpoint through relaxation techniques. In Table 2, we list the squared oscillation eigenfrequencies $\omega_n^2$ and overlap integrals $|Q_{nl}|$ for the f-mode and p-modes up to $p_5$, for both $l = 2$ and $l = 3$ modes, using the same conventions found in Lee and Ostriker (1986), which agree with those found here as well.

The tidal energy dissipation during an encounter can be expressed in the parameterized form given by Eq. (2.1) of Lee and Ostriker (1986), noting that in their first term, the superscript "2" was incorrectly transposed outside the parentheses,

$$\Delta E_p = \left( G M_*^2 / R_P \right) \sum_l \left( \frac{R_P}{r_p} \right)^{2l+2} T_l(\eta),  \qquad (B.1)$$

where the dimensionless separation parameter $\eta$ is defined by Eq. (13). Full details, including the derivation of the energy loss formula, can be found in Press and Teukolsky (1977) and Lee and Ostriker (1986). In Fig. 10, we show the dependence of $T_l(\eta)$ on $\eta$, for $l = 2$ and $l = 3$ using both of the polytropic EOS discussed above. We note in passing

Table 2
Squared oscillation eigenfrequencies and overlap integrals

| Mode | $(\omega^2)_{l=2}$ | $(|Q_{nl}|)_{l=2}$ | $(\omega^2)_{l=3}$ | $(|Q_{nl}|)_{l=3}$ |
|---|---|---|---|---|
| $n = 1.0$, $\Gamma_1 = 2.0$ | | | | |
| $f$ | 1.505 | 5.558E−1 | 2.884 | 5.845E−1 |
| $p_1$ | 11.98 | 2.689E−2 | 15.79 | 4.053E−2 |
| $p_2$ | 29.32 | 2.610E−3 | 35.61 | 4.294E−3 |
| $p_3$ | 52.68 | 3.128E−4 | 61.56 | 5.352E−4 |
| $p_4$ | 81.85 | 4.007E−5 | 93.38 | 7.113E−5 |
| $p_5$ | 116.7 | 4.699E−6 | 130.9 | 9.319E−6 |
| $n = 0.5$, $\Gamma_1 = 3.0$ | | | | |
| $f$ | 1.097 | 6.236E−1 | 2.230 | 7.093E−1 |
| $p_1$ | 18.50 | 6.613E−3 | 24.14 | 1.178E−2 |
| $p_2$ | 47.36 | 5.895E−4 | 57.64 | 5.594E−4 |
| $p_3$ | 86.33 | 3.780E−4 | 101.3 | 3.138E−4 |
| $p_4$ | 135.2 | 3.072E−4 | 155.0 | 2.669E−4 |
| $p_5$ | 193.9 | 2.569E−4 | 218.5 | 2.254E−4 |

*Note.* Dimensionless squared oscillation eigenfrequencies $\omega^2$ and overlap integrals $|Q_{nl}|$ for the $l = 2$ and $l = 3$ modes of polytropic models, defined in Eqs. (2.3)–(2.7) of Lee and Ostriker (1986). Units are such that $G = M_P = R_P = 1$, as used throughout.
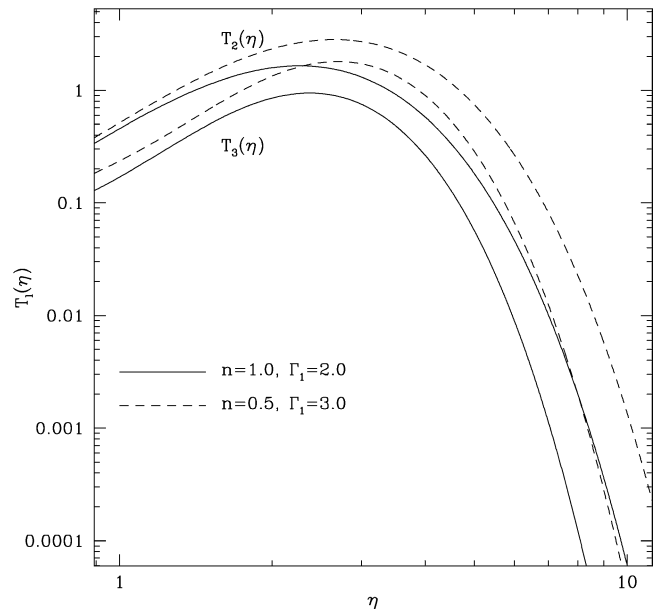


Fig. 10. Tidal energy transfer parameters $T_2(\eta)$ and $T_3(\eta)$, as functions of the interaction strength $\eta$, defined by Eq. (13), for polytropic models with $n = 1.0$, $\Gamma = 2.0$ (solid lines) and $n = 0.5$, $\Gamma_1 = 3.0$ (dashed lines), computed from Eq. (2.1) of Lee and Ostriker (1986). Note that in Lee and Ostriker (1986), the labels in Fig. 1a are reversed for the $l = 2$ and $l = 3$ modes.

that these curves are qualitatively similar to the $n = 3/2$ case shown in Fig. 1a of Lee and Ostriker (1986), who *reversed* the labels for the $l = 2$ and $l = 3$ mode on their figure; in general, $l = 2$ modes are almost always stronger for almost any physical system of interest. Since there are no low-frequency g-modes for these models, we see the expected exponential drop-off at larger separations. The largest contribution to all the cases shown here comes from the f-mode, which has the lowest frequency and is thus most coherently driven by the relatively long period interaction.

# References

Adams, F.C., Laughlin, G., 2003. Migration and dynamical relaxation in crowded systems of giant planets. Icarus 163, 290–306.

Balsara, D.S., 1995. von Neumann stability analysis of smooth particle hydrodynamics—suggestions for optimal algorithms. J. Comput. Phys. 121, 357–372.

Binney, J., Tremaine, S., 1987. Galactic Dynamics. Princeton Univ. Press, Princeton, NJ.

Bodenheimer, P., Lin, D.N.C., Mardling, R.A., 2001. On the tidal inflation of short-period extrasolar planets. Astrophys. J. 548, 466–472.

Bodenheimer, P., Laughlin, G., Lin, D.N.C., 2003. On the radii of extrasolar giant planets. Astrophys. J. 592, 555–563.

Boss, A.P., 1986. Protoearth mass shedding and the origin of the Moon. Icarus 66, 330–340.

Bouchy, F., Pont, F., Santos, N.C., Melo, C., Mayor, M., Queloz, D., Udry, S., 2004. Two new "very hot Jupiters" among the OGLE transiting candidates. Astron. Astrophys. 421, L13–L16.

Burrows, A., Sudarsky, D., Hubbard, W.B., 2003. A theory for the radius of the transiting Giant Planet HD 209458b. Astrophys. J. 594, 545–551.

Burrows, A., Hubeny, I., Hubbard, W.B., Sudarsky, D., Fortney, J.J., 2004. Theoretical radii of transiting giant planets: the case of OGLE-TR-56b. Astrophys. J. 610, L53–L56.

Butler, P., Vogt, S.S., Marcy, G.W., Fischer, D.A., Wright, J.T., Henry, G.W., Laughlin, G., Lissauer, J., 2004. A Neptune-mass planet orbiting the nearby M Dwarf GJ 436. Astrophys. J. 617, 580–588.

Chabrier, G., Barman, T., Baraffe, I., Allard, F., Hauschildt, P., 2004. The evolution of irradiated planets. Application to transits. Astrophys. J. 603, L53–L56.

Dintrans, B., Ouyed, R., 2001. On Jupiter's inertial mode oscillations. Astron. Astrophys. 375, L47–L50.

Dziembowski, W.A., 1971. Nonradial oscillations of evolved stars. I. Quasiadiabatic approximation. Acta Astronom. 21, 289–306.

Eggleton, P.P., 1983. Approximations to the radii of Roche lobes. Astrophys. J. 268, 368–369.

Evans, C.R., Kochanek, C.S., 1989. The tidal disruption of a star by a massive black hole. Astrophys. J. 346, L13–L16.

Faber, J.A., Rasio, F.A., 2000. Post-Newtonian SPH calculations of binary neutron star coalescence: method and first results. Phys. Rev. D 62, 064012.

Faber, J.A., Rasio, F.A., 2002. Post-Newtonian SPH calculations of binary neutron star coalescence. III. Irrotational systems and gravitational wave spectra. Phys. Rev. D 65, 084042.

Fabian, A.C., Pringle, J.E., Rees, M.J., 1975. Tidal capture formation of binary systems and X-ray sources in globular clusters. Mon. Not. R. Astron. Soc. 172, 15P–18P.

Ford, E.B., Rasio, F.A., Sills, A., 1999. Structure and evolution of nearby stars with planets. I. Short-period systems. Astrophys. J. 514, 411–429.

Ford, E.B., Havlickova, M., Rasio, F.A., 2001. Dynamical instabilities in extrasolar planetary systems containing two giant planets. Icarus 150, 303–313.

Gaudi, B.S., 2003. Extremely close-in giant planets from tidal capture. Astrophys. J. ArXiv Astrophysics e-prints. astro-ph/0307280.

Gu, P., Lin, D.N.C., Bodenheimer, P.H., 2003. The effect of tidal inflation instability on the mass and dynamical evolution of extrasolar planets with ultrashort periods. Astrophys. J. 588, 509–534.

Gu, P., Bodenheimer, P.H., Lin, D.N.C., 2004. The internal structural adjustment due to tidal heating of short-period inflated giant planets. Astrophys. J. 608, 1076–1094.

Guillot, T., Showman, A.P., 2002. Evolution of "51 Pegasus b-like" planets. Astron. Astrophys. 385, 156–165.

Hubbard, W.B., 1975. Gravitational field of a rotating planet with a polytropic index of unity. Sov. Astron. 18, 621–624.

Ivanov, P.B., Papaloizou, J.C.B., 2004a. On equilibrium tides in fully convective planets and stars. Mon. Not. R. Astron. Soc. 353, 1161–1175.

Ivanov, P.B., Papaloizou, J.C.B., 2004b. On the tidal interaction of massive extrasolar planets on highly eccentric orbits. Mon. Not. R. Astron. Soc. 347, 437–453.

Jeans, J.H., 1919. Problems of Cosmogony and Stellar Dynamics. Cambridge Univ. Press, Cambridge.

Kluzniak, W., Lee, W.H., 1998. Simulations of binary coalescence of a neutron star and a black hole. Astrophys. J. 494, L53–L55.

Konacki, M., Torres, G., Sasselov, D.D., Pietrzyński, G., Udalski, A., Jha, S., Ruiz, M.T., Gieren, W., Minniti, D., 2004. The transiting extrasolar giant planet around the Star OGLE-TR-113. Astrophys. J. 609, L37–L40.

Kuchner, M.J., Lecar, M., 2002. Halting planet migration in the evacuated centers of protoplanetary disks. Astrophys. J. 574, L87–L89.

Kumar, P., Goodman, J., 1996. Nonlinear damping of oscillations in tidal-capture binaries. Astrophys. J. 466, 946–956.

Kumar, P., Ao, C.O., Quataert, E.J., 1995. Tidal excitation of modes in binary systems with applications to binary pulsars. Astrophys. J. 449, 294.

Lacy, J.H., Townes, C.H., Hollenbach, D.J., 1982. The nature of the central parsec of the Galaxy. Astrophys. J. 262, 120–134.

Lai, D., Rasio, F.A., Shapiro, S.L., 1993. Ellipsoidal figures of equilibrium. Compressible models. Astrophys. J. Suppl. 88, 205–252.

Ledoux, P., Walraven, T., 1958. Variable stars. Handbuch der Physik 51, 353–604.

Lee, H.M., Ostriker, J.P., 1986. Cross sections for tidal capture binary formation and stellar merger. Astrophys. J. 310, 176–188.

Lin, D.N.C., Ida, S., 1997. On the origin of massive eccentric planets. Astrophys. J. 477, 781–791.

Lubow, S.H., Tout, C.A., Livio, M., 1997. Resonant tides in close orbiting planets. Astrophys. J. 484, 866–870.

Luminet, J.-P., Carter, B., 1986. Dynamics of an affine star model in a black hole tidal field. Astrophys. J. Suppl. 61, 219–248.

Marzari, F., Weidenschilling, S.J., 2002. Eccentric extrasolar planets: the jumping Jupiter model. Icarus 156, 570–579.

Mayor, M., Udry, S., Naef, D., Pepe, F., Queloz, D., Santos, N.C., Burnet, M., 2004. The CORALIE survey for southern extra-solar planets. XII. Orbital solutions for 16 extra-solar planets discovered with CORALIE. Astron. Astrophys. 415, 391–402.

McArthur, B.E., Endl, M., Cochran, W.D., Benedict, G.F., Fischer, D.A., Marcy, G.W., Butler, R.P., Naef, D., Mayor, M., Queloz, D., Udry, S., Harrison, T.E., 2004. Detection of a Neptune-mass planet in the $\rho^1$ Cancri system using the Hobby–Eberly telescope. Astrophys. J. 614, L81–L84.

Ogilvie, G.I., Lin, D.N.C., 2004. Tidal dissipation in rotating giant planets. Astrophys. J. 610, 477–509.

Paczyński, B., 1971. Evolutionary processes in close binary systems. Annu. Rev. Astron. Astrophys. 9, 183–208.

Press, W.H., Teukolsky, S.A., 1977. On formation of close binaries by two-body tidal capture. Astrophys. J. 213, 183–192.

Rasio, F.A., Ford, E.B., 1996. Dynamical instabilities and the formation of extrasolar planetary systems. Science 274, 954–956.

Rasio, F.A., Shapiro, S.L., 1992. Hydrodynamical evolution of coalescing binary neutron stars. Astrophys. J. 401, 226–245.

Rasio, F.A., Tout, C.A., Lubow, S.H., Livio, M., 1996. Tidal decay of close planetary orbits. Astrophys. J. 470, 1187–1191.

Rees, M.J., 1988. Tidal disruption of stars by black holes of 10 to the 6th–10 to the 8th solar masses in nearby galaxies. Nature 333, 523–528.

Sasselov, D.D., 2003. The new transiting Planet OGLE-TR-56b: orbit and atmosphere. Astrophys. J. 596, 1327–1331.

Saumon, D., Hubbard, W.B., Burrows, A., Guillot, T., Lunine, J.I., Chabrier, G., 1996. A theory of extrasolar giant planets. Astrophys. J. 460, 993–1018.

Sills, A., Faber, J.A., Lombardi, J.C., Rasio, F.A., Warren, A.R., 2001. Evolution of stellar collision products in globular clusters. II. Off-axis collisions. Astrophys. J. 548, 323–334.

Torres, G., Konacki, M., Sasselov, D.D., Jha, S., 2004. New data and improved parameters for the extrasolar transiting Planet OGLE-TR-56b. Astrophys. J. 609, 1071–1075.

Trilling, D.E., Benz, W., Guillot, T., Lunine, J.I., Hubbard, W.B., Burrows, A., 1998. Orbital evolution and migration of giant planets: modeling extrasolar planets. Astrophys. J. 500, 428–439.

Weidenschilling, S.J., Marzari, F., 1996. Gravitational scattering as a possible origin for giant planets at small stellar distances. Nature 384, 619–621.